Geotextiles and Geomembranes 50 (2022) 1052–1059

Contents lists available at ScienceDirect

Geotextiles and Geomembranes

journal homepage: www.elsevier.com/locate/geotexmem

Influence of asphalt thickness on performance of geosynthetic-reinforced asphalt: Full-scale field study

V. Vinay Kumar [a,*], Gholam H. Roodi [b], S. Subramanian [a], Jorge G. Zornberg [a]

[a] Department of Civil, Architectural and Environmental Engineering, University of Texas at Austin, Austin, TX, 78712, USA
[b] HDR, Toronto, Ontario, Canada

ARTICLE INFO

Keywords:
Geosynthetics
Asphalt overlay
Instrumentation
Field monitoring
Tensile strains
Structural capacity

ABSTRACT

In this study, a series of controlled traffic loadings was conducted on unreinforced and geosynthetic-reinforced full-scale asphalt overlays. Unlike the common objective of using paving interlayers to mitigate the development of reflective cracks, the main purpose of adopting geosynthetics for this study was to render an increased roadway structural capacity. The project involved instrumented test sections constructed during the rehabilitation of an in-service roadway in Texas, USA. The rehabilitation involved repairing the pre-existing pavement, placing tack coat, installing a geosynthetic interlayer (except in the unreinforced section), and finally constructing a 75 mm-thick asphalt overlay. This overlay comprised a 50 mm-thick, dense-graded (TY-D) layer overlain by a 25 mm-thick, thin-overlay mixture (TOM) layer. Controlled traffic loadings were conducted, which involved driving standard and light axle loads directly above asphalt strain gauges that had been installed at mid-depth of the pre-existing asphalt layer. Comparison of tensile strains among the different test sections revealed significantly smaller tensile strains in the geosynthetic-reinforced sections compared to those obtained in the unreinforced section. Consequently, and even though geosynthetic interlayers have often been adopted to minimize reflective cracking in asphalt overlays, the field monitoring results generated in this study demonstrate that they also provide added roadway structural capacity.

1. Introduction and background

Several types of geosynthetics, collectively known as paving interlayers but involving different materials (e.g., polymers, glass) and various forms (e.g., geotextiles, geogrids, geocomposites), have been widely adopted as anti-reflective cracking systems during the construction of asphalt overlays. In addition to mitigating the development of reflective cracks, some of these paving interlayers have been speculated to also provide increased structural capacity. However, information about such additional benefit has been largely anecdotal as systematic field evaluation of this benefit has remained largely unquantified. Geosynthetic interlayers have been generally installed below the asphalt overlays and may achieve the goal of retarding or minimizing reflective cracks through mechanisms that involve functions such as separation, reinforcement, and barrier (Elseifi 2003; Ferrotti et al., 2012; Zornberg 2017). Specifically, paving interlayers generally involving geotextile products have been reported to minimize reflective cracking by providing a separation function between the pre-existing and new asphalt layers through a stress-relief mechanism (Lytton 1989; Zornberg 2017; Solatiyan et al., 2020). Instead, paving interlayers generally involving geogrid products have been reported to minimize reflective cracking by providing a reinforcement function to reduce the stress concentration that triggers reflective cracks (Zornberg 2017; Solatiyan et al., 2020; Kumar et al., 2021a). Finally, paving interlayers involving geocomposites have been reported to behave similar to geogrids in minimizing reflective cracks but often also provide a barrier function (Pasquini et al., 2014; Zornberg 2017; Solatiyan et al., 2020). Some paving fabrics are also expected to provide the barrier function along with separation (Lytton 1989; Farshad 2005). While the original motivation for the development of the various paving interlayer products has been to mitigate reflective crack development, preliminary investigations conducted by Correia and Zornberg (2016, 2018) and Kumar et al. (2021b) suggest that the reinforcement mechanisms developed by geogrids may also lead to an increased structural capacity of the reinforced overlays. Specifically, the inclusion of geogrid reinforcements below the asphalt overlay may minimize the accumulation

* Corresponding author. 301, E. Dean Keeton St., ECJ 9.236, Austin, TX, 78712, USA.
E-mail addresses: vinay.vasanth@utexas.edu (V.V. Kumar), gholamhossein.roodi@hdrinc.com (G.H. Roodi), ssubu.ind@utexas.edu (S. Subramanian), zornberg@mail.utexas.edu (J.G. Zornberg).

https://doi.org/10.1016/j.geotexmem.2022.06.005
Received 5 December 2021; Received in revised form 26 May 2022; Accepted 15 June 2022
Available online 5 July 2022

of permanent deformations and critical tensile strains under repeated traffic and environmental loads. While such increased structural capacity would be highly beneficial, the lack of field monitoring results that quantify such structural benefit has precluded the incorporation of added capacity in roadway design.

The efficacy of various types of geosynthetic interlayers in enhancing the overlay performance against reflective cracking has been evaluated by several researchers (Lytton 1989; Cleveland et al., 2002; Virgili et al., 2009; Zamora-Barraza et al., 2011; Pasquini et al., 2014; Gonzalez-Torre et al., 2015; Kumar and Saride 2017; Sudarsanan et al., 2019). A wide range of experimental procedures have been adopted to quantify the crack development in the laboratory, including conducting flexural beam fatigue tests (e.g., Virgili et al., 2009; Kumar and Saride 2017; Saride and Kumar 2017, 2019; Solatiyan et al., 2021), bond strength tests (e.g., West et al., 2005; Roodi et al., 2017; Saride and Kumar 2017; Solatiyan et al., 2021; Spadoni et al., 2021; Canestrari et al., 2022), and pavement model tests (e.g., Sanders 2001; Siriwardane et al., 2010; Correia and Zornberg 2016; Saride and Kumar 2019; Kumar et al., 2021b). Complementing the insight gained from experimental research, field investigations involving both unreinforced and geosynthetic-reinforced asphalt overlays have also been performed to evaluate the efficacy of geosynthetic interlayers to control reflective cracking (e.g., Laurinavicius and Oginskas 2006; Buhler 2007; Graziani et al., 2014; Imjai et al., 2019; Kumar et al., 2021c). Finally, a number of researchers have resorted to numerical simulations such as the finite element method (FEM) to evaluate the efficacy of geosynthetics in minimizing reflective cracks (e.g., Wathugala et al., 1996; Kwon et al., 2005; Abdesssemed et al., 2015; Correia et al., 2018; Kazimierowicz--Frankowska 2020). However, the results from various laboratory scale tests, pavement model tests, field trials, and numerical simulations reveal consensus on the benefits, but not on the mechanisms by which geosynthetic interlayers minimize the development of reflective cracks in the asphalt overlays. In summary, and in spite of the possible lack of consensus on the relevant mechanisms, previous research on geosynthetic-reinforced asphalt overlays is available, but it has emphasized quantifying their ability to restrict reflective cracks into the asphalt overlays. On the other hand, limited experimental research has been generated on the potential structural benefits of incorporating geosynthetic reinforcements within the asphaltic layers (e.g., Correia and Zornberg 2016, 2018; Kumar et al., 2021b). In addition, a few full-scale field studies have been conducted that report on the structural benefits of incorporating the geosynthetics between the asphalt overlays (e.g., Laurinavicius and Oginskas 2006; Graziani et al., 2014; Imjai et al., 2019). However, the field evaluations conducted by Laurinavicius and Oginskas (2006) did not include any sensors, while field evaluations conducted by Graziani et al. (2014) and Imjai et al. (2019) included sensors (i.e., asphalt strain gages, and pressure sensors), but the geosynthetic interlayers were installed within new asphalt layers instead of a typical geosynthetic installation viz. below an asphalt overlay. Also, none of the previous full-scale field studies have evaluated the influence of different asphalt thicknesses on the structural performance of geosynthetic-reinforced asphalt overlays. Consequently, a research program involving evaluation of the structural performance of full-scale instrumented field sections was implemented in this study to quantify the structural benefits expected from geosynthetics placed below the asphalt overlay, but not necessarily benefits against reflective cracking. Specifically, the field study presented in this research provides an evaluation of the influence of two different asphalt thickness with different asphalt types, on the performance of full-scale highway sections with unreinforced and geosynthetic-reinforced asphalt overlays under a series of controlled traffic loadings. The performance of each geosynthetic-reinforced section is compared against that of the control section, allowing quantification of the structural benefits derived from geosynthetic reinforcement. Specifically, reductions in tensile strain due to geosynthetic reinforcements are quantified for two different overlay thicknesses. The influence of overlay types is also qualitatively evaluated. Field loading campaigns were conducted as part of this study at locations where the pre-existing asphalt was intact. Consequently, rather than focusing on the impact of mitigating reflective cracking, the differences in performance between reinforced and control sections allow quantification of the impact of the geosynthetic reinforcements on the roadway structural capacity.

2. Materials and methods

2.1. Road profile and sensor instrumentation

A 32 km stretch of in-service State Highway (SH) 21 in Texas, US was rehabilitated by the State transportation agency (TxDOT) to restore roadway serviceability. The rehabilitation program included treatment of distresses in the pre-existing asphalt surface, application of tack coat, installation of the geosynthetic reinforcement (except in the unreinforced sections), and construction of a 75 mm-thick asphalt overlay. A section of this highway rehabilitation project was selected to investigate the effectiveness of different geosynthetic interlayers adopted as asphalt reinforcement in this study. In this regard, four test sections described in this study (one unreinforced and three reinforced sections) are among those instrumented with multiple asphalt strain gauges (ASG). They included duplicate gauges installed in the wheel path, gauges oriented to measure strains transverse to the direction of the wheel path (i.e., maximum horizontal tensile strains). The collected strain information is relevant because the accumulation of horizontal tensile strains at the bottom of the asphalt layer ultimately results in fatigue cracking. The tensile strain data reported in this study corresponds to one of the two duplicate sensors in each of the four test sections, while the data from the other sensor was used for validation purposes. It should be noted that the ASGs used in this study have been successfully used in asphalt layers in previous studies and found to be highly reliable (e.g., Graziani et al., 2014; Correia and Zornberg 2016, 2018). Fig. 1 presents a typical road profile (cross-section) of the full-scale instrumented test section. As indicated in the figure, the thickness of the unbound aggregate (base and subbase) layer and the pre-existing asphalt layers were 375 mm and 150 mm, respectively. The thickness of pre-existing pavement layers was confirmed by coring through pavement layers in the four test sections. In addition, GPR surveys were also performed on the pre-existing asphalt surface to determine pre-existing conditions such as the thickness of different pavement layers. The ASGs were installed at mid-depth (75 mm) of the pre-existing asphalt layer, which involved drilling holes to the required depth, cleaning and placing a thin layer of fine sand-bitumen mixture at the bottom of the holes as shown in Fig. 2. A dense-graded asphalt mixture (TY-D) was used to fill the core after the ASG installation. After evaluating multiple field installation protocols, the sensor installation technique ultimately adopted in this study involved two 125 mm dia. holes drilled 25 mm apart and connected via a 25 mm slit (Fig. 2), as this approach was found to effectively minimize sensor damages during their installation and subsequent overlay construction process. The H-shaped ASGs (see Fig. 2) adopted in this study comprised two metal flanges connected by a polymeric-web that encased four 350 Ω strain gauges in full-bridge configuration for axial strain measurements. The strain gauges could withstand the high temperatures expected during the hot mix asphalt placement and were coated with bitumen to enhance their bonding with the surrounding asphalt. The asphalt overlay for the SH21 project involved a 50 mm-thick dense-graded asphalt mixture (TY-D) layer (see Fig. 1a) overlain by a 25 mm-thick wearing-course asphalt mixture (TOM) layer (see Fig. 1b). The asphalt mixtures (TY-D and TOM) were adopted according to Texas Department of Transportation (TxDOT) standard specifications for construction and maintenance of highways, streets, and bridges (TxDOT 2014).

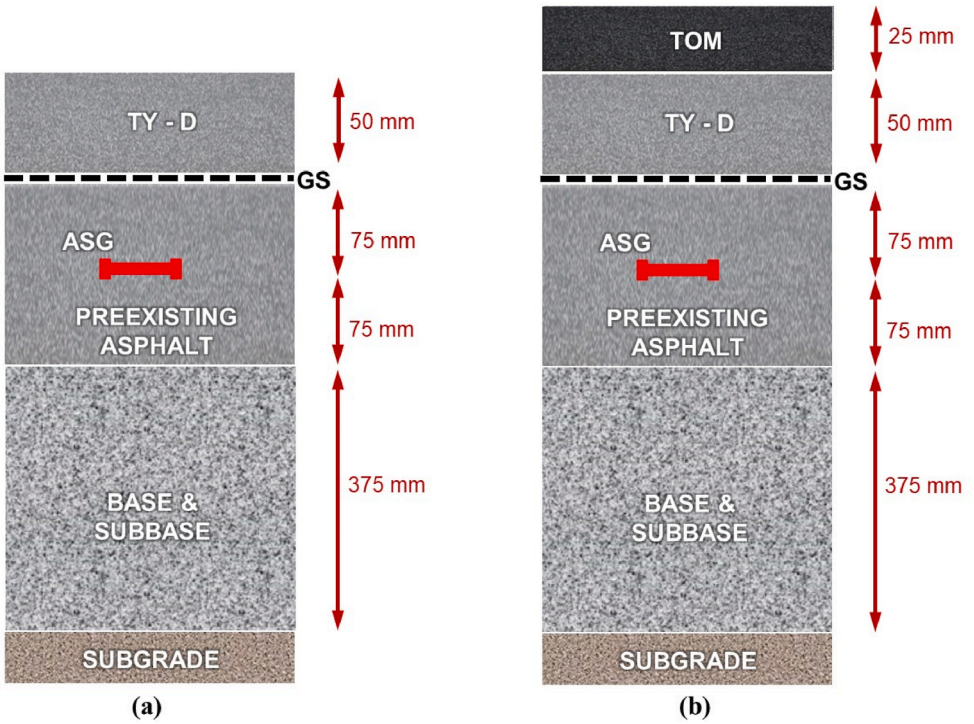

Fig. 1. Road profile showing location of ASG sensors in the test sections: (a) Pavement Configuration A; and (b) Pavement Configuration B.

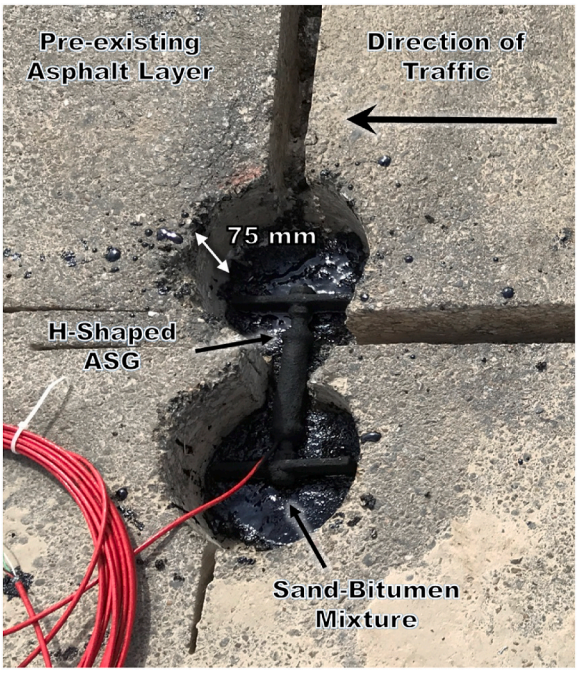

Fig. 2. Typical asphalt strain gage installed in the mid-depth of pre-existing asphalt layer.

2.2. Geosynthetic reinforcements

Three different types of geosynthetic interlayers, representative of products that have been commonly used as reinforcement interlayers, namely a polyester (PET) geogrid composite, a polyvinyl alcohol (PVA) geogrid composite, and a fiberglass geogrid composite were adopted in this study for asphalt reinforcement. While the variety of geosynthetic interlayers is significant, this study did not focus on other interlayer functions or mechanisms such as barrier or stress relief. In addition, all three products were selected from the same manufacturer, considering their material composition, tensile and physical characteristics. The product identified herein as GS-1 is a geogrid manufactured with high modulus polyester yarns combined with an ultra-light non-woven fabric. Product GS-2 is a geogrid manufactured using polyvinyl alcohol, also combined with an ultra-light non-woven fabric. These two polymeric interlayers are coated with a binder to enhance their bonding with the adjacent asphalt layers. The third product, GS-3, is a geogrid made of glass fibers combined with an ultra-thin non-woven fabric and coated with a binder. Table 1 summarizes the manufacturer-reported physical and mechanical properties of the geosynthetic interlayers adopted in this study.

2.3. Asphalt mixture and tack coat

Two different types of asphalt mixtures were used as asphalt overlays in this project, including a dense-graded asphalt mixture, referred to as TY-D, and a thin wearing-course asphalt mixture referred to as TOM. Fig. 3 presents the gradation curves for the asphalt mixtures adopted in this study. As shown in the figure, the maximum aggregate sizes in the TY-D and TOM mixtures were 20 mm and 12.5 mm, respectively. The TY-D mixture involved a Performance Grade (PG) 64-22 binder at an optimum binder content of 5.2%, while the TOM corresponded to a PG 76-22 binder at an optimum binder content of 6%. In addition, a warm mix additive (Evotherm) was added at a rate of 0.4% by weight of aggregates for use as a compaction aid in both asphalt mixtures.

The tack coat types and application rates were not necessarily the same for the different geosynthetic reinforcements. This is because the tack coat type and rate recommended by each manufacturer and consistent with TxDOT's available specifications was adopted. A polymer modified asphalt cement (AC-15P) was applied during construction of the geosynthetic-reinforced test sections using a tack coat rate of 0.54 l/m^2 over the pre-existing asphalt layer. The geosynthetic interlayers were subsequently installed, and the TY-D asphalt layer was ultimately placed and compacted. In the control section, a cationic, slow-setting,

Table 1
Manufacturer-reported Physical and Mechanical Properties of Geosynthetic Reinforcements adopted in this study.

Property	Test Method	Polyester Geogrid Composite (GS-1)	Polyvinyl Alcohol Geogrid Composite (GS-2)	Fiberglass Geogrid Composite (GS-3)
Mass/unit area	ASTM D5261	270 g/m^2	210 g/m^2	596 g/m^2
Aperture size	Measured	40 mm × 40 mm	40 mm × 40 mm	30 mm × 30 mm
Tensile strength MD	ASTM D6637	50 kN/m	50 kN/m	100 kN/m
CMD	ASTM D6637	50 kN/m	50 kN/m	100 kN/m
Unit tension at 3% strain	ASTM D6637	12 kN/m	25 kN/m	–
Elongation at failure	ASTM D6637	≤10%	≤5%	<3%
Asphalt retention capacity	ASTM D6140	0.47 l/m^2	0.47 l/m^2	0.47 l/m^2
Melting point	ASTM D276	255 °C	230 °C	>800 °C
Shrinkage at 190 °C for 15 min		<1%	<1%	<1%

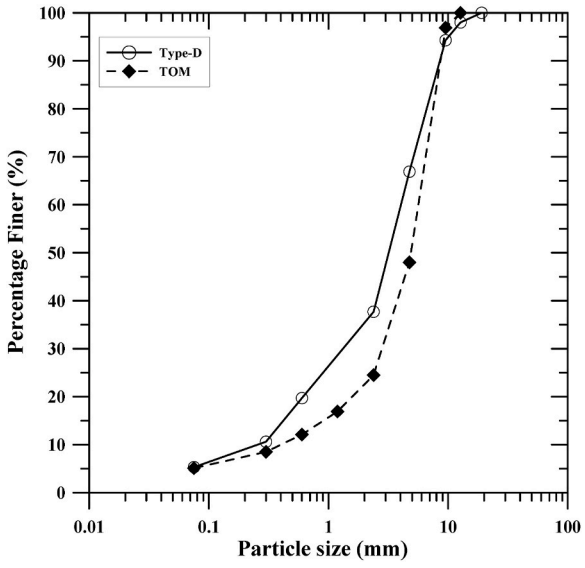

Fig. 3. Gradation curves for TY-D and TOM asphalt mixtures adopted in the study.

low-viscosity, comparatively hard residue emulsion (CSS–1H) was applied at a rate of 0.27 l/m^2 over the pre-existing asphalt layer before placing and compacting the TY-D asphalt layer. The emulsion CSS-1H was applied at a rate of 0.27 l/m^2 as tack coat between the TY-D and TOM asphalt layers during construction of all test sections, as such selected emulsion facilitated trafficability of construction vehicles over the exposed tack coated surface.

2.4. Controlled traffic loading campaigns

The effect on the overlay performance of the asphalt overlay type and thickness as well as of the selected geosynthetic interlayers were evaluated using field data collected as part of controlled traffic loading campaigns performed in the four test sections considered in this study. Specifically, controlled traffic loadings were performed on the four instrumented test sections after construction of the 50 mm-thick TY-D layer, referred to as Pavement Configuration A (see Fig. 1a). In addition, controlled traffic loadings were conducted after construction of the 25 mm-thick TOM layer, referred to as Pavement Configuration B (see Fig. 1b). Each controlled traffic loading involved multiple passes (typically 10 passes) of a heavy truck (standard axle load) as well as of a passenger car (light axle load), both with known weights. The wheel load and tire pressures for both heavy truck and passenger car were measured using a load cell and a pressure cell during each controlled traffic loading campaign. The vehicles were driven directly over the sensor locations at an average speed of 40 kph during the loadings conducted on Pavement Configurations A and B in the four test sections considered in this study. The tensile strain responses induced by the traffic loading were recorded by the asphalt strain gauges embedded in the pre-existing asphalt layer. The tensile strain readings were set to zero before the pass of each standard and light axle loading to allow measurement of the peak tensile strain induced by each individual axle loading. In addition, GoPro cameras were mounted on the truck and car during the loading campaigns to capture their wheel path (see Fig. 4a) relative to the location of ASGs installed in the transverse direction (i.e., perpendicular to the traffic direction) as shown in Fig. 4b to c. Such information from the cameras helped in differentiating passes that were directly above the sensors from imprecise passes. The tensile strain results recorded from the four test sections considered in this study are discussed in the following sections.

3. Results and discussion

3.1. Tensile strain response under controlled traffic loadings

Typical tensile strain results obtained in the control section for multiple standard and light axle loadings on Pavement Configuration A (see Fig. 1a) are presented in Fig. 5a and b, respectively. As shown in the figures, the tensile strain trends for the various passes are similar, and as expected, the peak tensile strains recorded under standard axle loads were consistently higher than those recorded under light axle loads. For instance, a peak tensile strain of 650 μm/m (see Fig. 5a) was recorded under a standard axle load with a load of 30.25 kN per wheel that had a tire pressure of 550 kPa and a contact area of 0.055 m^2. On the other hand, the peak tensile strain recorded under a light axle load (4.67 kN per wheel) with a tire pressure of 250 kPa and a contact area of 0.019 m^2, was about 165 μm/m (see Fig. 5b), which is approximately four times lower than the tensile strain recorded under the standard axle load. Ultimately, the magnitude of the tensile strain for the different loadings depends on the applied load, contact pressure and the loading area. The strain results presented in Fig. 5a and b correspond to a short time window (0.2 s) that includes the duration of direct contact of the moving standard and light axle loads directly over the sensors.

The peak tensile strains recorded from multiple passes during the loadings were compared to determine the maximum peak tensile strain value among the multiple passes. Such maximum peak tensile strain values for the four test sections subjected to standard axle loading are shown in Fig. 6 for Pavement Configurations A and B. Fig. 7 shows the results for the same test sections and overlay thicknesses but considering the light axle loading. It is apparent that the tensile strains in the control section are consistently higher than those in the three geosynthetic-reinforced sections, irrespective of the overlay thickness (Pavement Configurations A and B) or the applied axle loads (Standard or light). For instance, the results in Fig. 6 indicate that a maximum tensile strain of 655 μm/m was reached in the control section, but significantly lower peak tensile strains were obtained in the geosynthetic-reinforced sections under standard axle loads applied to Pavement Configuration A (300 μm/m in GS-1, 250 μm/m in GS-2, and 350 μm/m in GS-3). This corresponds to reductions in tensile strain of approximately 54%, 62%, and 47% in geosynthetic-reinforced test sections GS-1, GS-2, and GS-3, respectively. These results show that the inclusion of geosynthetic

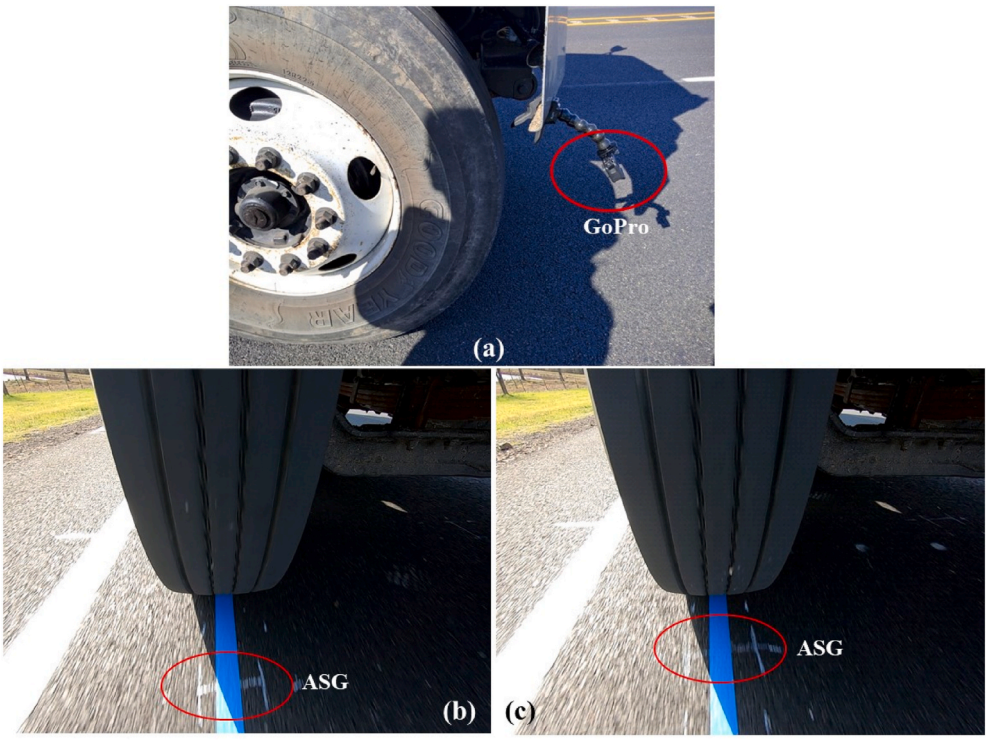

Fig. 4. Quality control during loading campaigns: (a) Camera mounted in front of the truck wheel; (b) Wheel location immediately before crossing an ASG in the transverse direction; and (c) Wheel location immediately before crossing a duplicated ASG in the transverse direction.

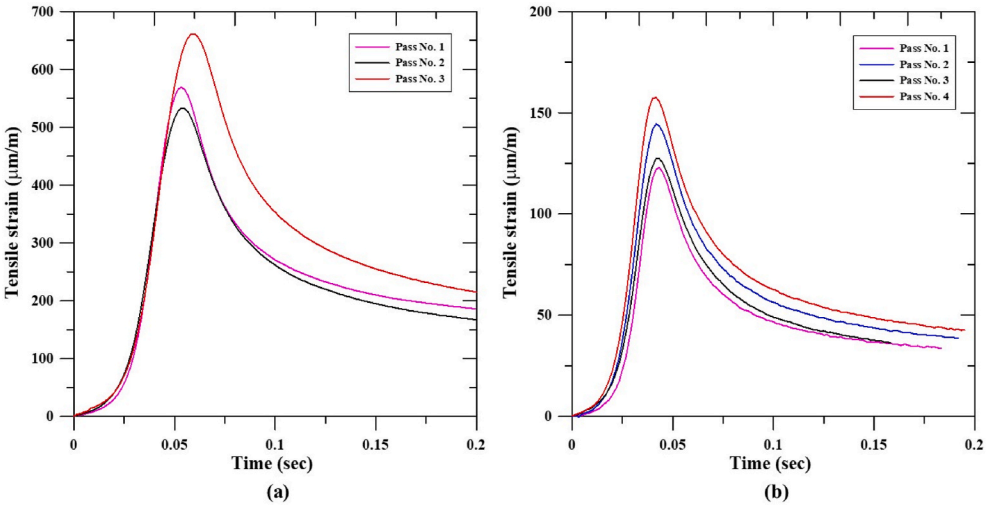

Fig. 5. Typical tensile strain response in Control Section for: (a) Standard axle load; and (b) Light axle loads applied on Pavement Configuration A.

interlayers considered in this study, when placed at the interface between the pre-existing and new asphalt layers are effective in reducing the tensile strains under traffic loads. Among the geosynthetic-reinforced sections, the tensile strain reductions in Section GS-2 were slightly higher than those in Section GS-1, which were in turn slightly higher than those in Section GS-3. Yet, the response of the three geosynthetic interlayers is deemed to be reasonably similar for the different products used in this field study in spite of their differences in tensile strength and stiffness. This observation suggests that properties other than the tensile strength and stiffness are relevant to the performance upon loading. In particular the interface bond strength is expected to significantly impact the performance of geosynthetic-reinforced sections. Trends similar to those observed for the standard axle loads were obtained due to light axle loading on Pavement Configuration A, as shown in Fig. 7.

On the other hand, the results shown in Figs. 6 and 7 also show the tensile strains in all the test sections considered in this study decrease with increasing asphalt thickness, irrespective of presence or not of geosynthetic reinforcements. For instance, as revealed by the results in Fig. 6, the tensile strains in the control section of Pavement Configuration A (655 μm/m) are significantly higher than those in the control section of Pavement Configuration B (75 μm/m), which corresponds to an approximate reduction of 89% in strains due to the additional overlay thickness of 25 mm (TOM layer). Similar trends can be observed in the case of geosynthetic-reinforced sections with about 80% reduction in strains due to the additional overlay thickness of 25 mm (TOM layer). However, the benefits (tensile strain reduction) due to geosynthetic reinforcements was approximately 60% smaller for Pavement

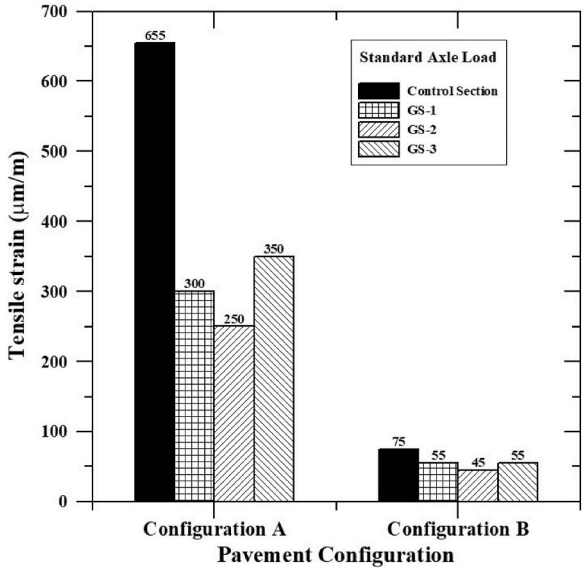

Fig. 6. Peak tensile strains in all the four test sections under Standard axle loads.

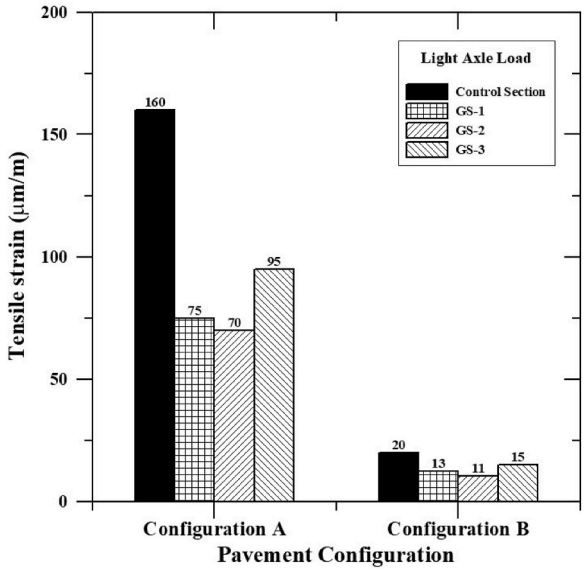

Fig. 7. Peak tensile strains in all the four test sections under Light axle load.

Configuration B in relation to Pavement Configuration A (i.e., with an additional 25 mm of TOM layer). Similar trends can be observed for the light axle loads applied on Pavement Configuration B as shown in Fig. 7. These trends also suggest that the benefit of adding a geosynthetic reinforcement depends on the actual thickness and quality of the asphalt overlay. Accordingly, a comparatively small benefit may be expected when using a comparatively thick, high quality asphalt layer, at least immediately after placement of the asphalt overlay. The benefit of using geosynthetic reinforcements will become more significant once the modulus of a comparatively thick asphalt overlay degrades with time. In the case of this study, the reduction in the tensile strains due to the presence of a geosynthetic reinforcement was more significant for the case of a comparatively thin (and lower quality) asphalt layer (i.e., a 50 mm-thick asphalt layer instead of a 75 mm-thick layer that includes a 25 mm-thick TOM layer). Adopting a comparatively thin layer of reinforced asphalt would not only result in reduced construction costs, but it would also lead to a more efficient geosynthetic reinforcement. On the other hand, the incorporation of geosynthetic interlayers in projects involving a comparatively thick layer of reinforced asphalt will still capitalize on the geosynthetic benefits, but only after degradation of the thick asphalt layer. It should be noted that, consistent with the results of this study, the optimum asphalt thickness also depends on the asphalt type (i.e., TOM vs TY-D in the case of this study). In addition, project-specific components (e.g., traffic loading, environmental conditions, pavement design life) would also affect the selection of the optimum asphalt thickness when accounting for the structural benefit of geosynthetic interlayers. It should be noted that the ambient air temperatures recorded at the time of the loadings of Pavement Configurations A in the four test sections (about 33 °C) were comparatively higher than those recorded during the loadings of Pavement Configuration B (about 13 °C). Table 2 presents a summary of the recorded ambient air temperatures in the four test sections during the loading campaigns of Pavement Configurations A and B. The differences among the recorded air temperatures during the different loading campaigns were deemed to be significant. On the other hand, the differences in temperature registered during a given loading campaign were deemed to be comparatively minor in spite of loading taking place over different test sections and using different axle loads.

As expected, the results in Fig. 7 indicate that the tensile strains recorded under light axle loads are lower than those recorded under standard axle loads, which is consistent with the evidences that fatigue damage is dominated by the heavy traffic loads. Consistent with the trends of results generated under standard axle loading, the tensile strain trends of results generated under light axle loading show more significant reductions in tensile strains in the geosynthetic-reinforced sections with a 50 mm-thick asphalt overlay (TY-D) than in the sections with a 75 mm-thick overlay (50 mm TY-D and 25 mm TOM). However, it should be highlighted that the three geosynthetic reinforcements evaluated in this study were effective in minimizing the tensile strains under both standard and light axle loads, leading to an enhanced performance of the pavement system. To further quantify the improvement in terms of tensile strain reductions in the three reinforced sections against the control section, the tensile strain reduction ratio is introduced as a performance indicator, as discussed in the following section.

3.2. Tensile strain reduction ratio

The tensile strain reduction ratio (α) is defined herein as the ratio between the peak tensile strain in a geosynthetic-reinforced section and that in the control section, irrespective of the applied loads and pavement configurations. Accordingly, a tensile strain reduction ratio of comparatively small magnitude represents an important reduction in tensile strain (i.e., improved performance corresponds to low 'α' values). It should be noted that the tensile strain reduction ratios for Pavement Configurations A and B were determined at temperatures of about 33 °C and 13 °C, respectively. Such tensile strain reduction ratios for the three geosynthetic-reinforced sections considered in this study are presented in Figs. 8 and 9 for the cases of standard and light axle loads, respectively. The results shown in the figures indicate that the tensile strain

Table 2
Summary of ambient air temperatures recorded during the loading of Pavement Configurations A and B.

Load condition	Test Sections	Ambient Air Temperature (°C)	
		Configuration A	Configuration B
Standard Axle	Control Section	34.3	14.1
	GS-1	33.2	13.6
	GS-2	33.2	10.4
	GS-3	34.3	14.1
Light Axle	Control Section	34.3	14.1
	GS-1	33.6	13.9
	GS-2	33.2	10.7
	GS-3	33.6	14.1

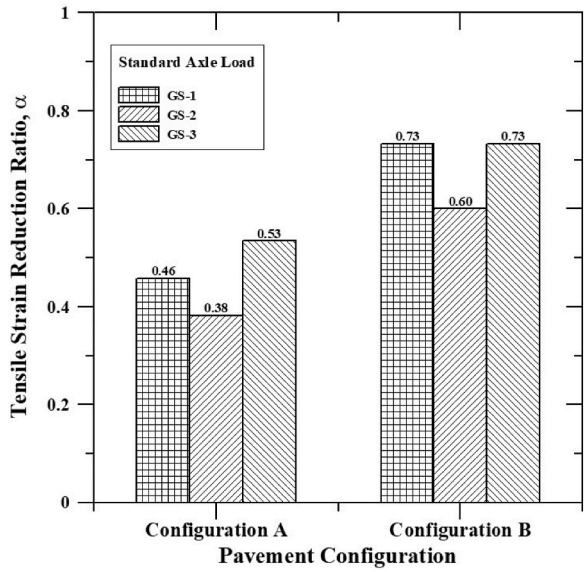

Fig. 8. Tensile strain reduction ratios for geosynthetic-reinforced test sections under Standard axle load.

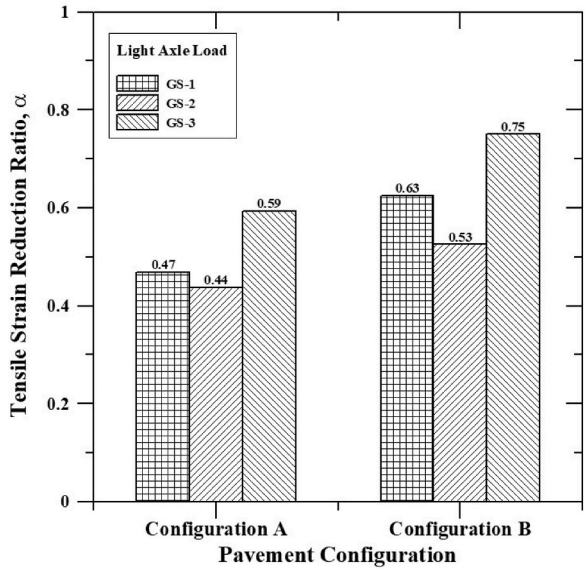

Fig. 9. Tensile strain reduction ratios for geosynthetic-reinforced test sections under Light axle load.

reduction ratios for loadings conducted on Pavement Configuration A are consistently smaller than the ratios corresponding to loadings conducted on Pavement Configuration B, irrespective of the magnitude of the applied axle loads. For instance, the tensile strain reduction ratios under standard axle loads shown in Fig. 8 range from 0.38 to 0.53 for Pavement Configuration A, but are higher (ranging from 0.60 to 0.73) for Pavement Configuration B. While, the tensile strain reduction ratios under light axle loads shown in Fig. 9 range from 0.44 to 0.59 for Pavement Configuration A and 0.53 to 0.75 for Pavement Configuration B. These results indicate that the tensile strain reduction ratios depend on the pavement configurations (i.e., thickness and type of the asphaltic layer), traffic load magnitudes and also the ambient air and asphalt temperatures during the loadings.

It should also be noted that reasonably similar tensile strain reduction ratios were obtained for the three geosynthetic-reinforced sections considered in this study. Yet, the variations in tensile strain reduction ratio among the geosynthetic-reinforced sections can be attributed primarily to the tensile strength, tensile stiffness and interface bonding of geosynthetic reinforcements (see Table 1). The stiffness of asphalt overlay may have also affected the magnitude of the tensile strain reduction ratios of the three geosynthetic-reinforced sections evaluated in this study. The benefits that result from using geosynthetic reinforcements appear to be maximized when the stiffness of asphalt layer is comparatively low. In the case of this study, since the stiffness of the 50 mm-thick asphalt layer (TY-D) is lower than the combined stiffness of the 75 mm-thick (50 mm TY-D and 25 mm TOM) asphalt layer; the benefits from adopting geosynthetic reinforcements were more prominent in Pavement Configuration A (50 mm-thick asphalt layer) than in Pavement Configuration B (75 mm-thick asphalt layer).

Overall, it can be inferred that all the geosynthetic-reinforced sections considered in this study showed a clearly superior structural capacity to that of the control section, as evidenced by the reduced tensile strains under standard and light axle loads applied to Pavement Configurations A and B. This finding may have significant practical implications, considering that geosynthetic interlayers are often selected in asphalt overlays with the objective of minimizing reflective cracking rather than increasing the structural capacity of the flexible pavement. While the future performance of the test sections also helps evaluating the effectiveness of the different geosynthetic interlayers to minimize reflective cracking, such evaluation is beyond the objectives of this study. The tensile strain reduction ratios obtained for 50 mm-thick (TY-D) and 75 mm-thick (50 mm TY-D and 25 mm TOM) asphalt overlays under standard and light axle loads indicate that the geosynthetic reinforcements were significantly more effective for comparatively thin asphalt overlays. The tensile strain reduction ratios determined from geosynthetic-reinforced sections considered in this study may be adopted as part of the pavement design to reduce the asphalt overlay thickness and/or extend the service life without compromising the overall performance of the pavement system. The performance of such a flexible pavement system with reduced thickness and an extended service life is expected to be ultimately verified under the framework of a Mechanistic-Empirical Pavement Design approach.

4. Conclusions

A series of controlled traffic loadings were conducted on full-scale instrumented field test sections comprising unreinforced and geosynthetic-reinforced asphalt overlays constructed in an in-service roadway (State Highway 21) in Texas, US. The impact of using geosynthetic interlayers on the structural capacity of the roadway was evaluated while accounting for the influence of asphalt thickness during controlled traffic loading campaigns conducted on unreinforced and geosynthetic-reinforced asphalt overlay sections. The following conclusions can be drawn from this study:

- The use of asphalt strain gauges, installed in this study at a depth of 75 mm within the pre-existing asphalt layer in four test sections, were found to effectively measure the tensile strains under the controlled traffic loadings conducted in this study.
- As expected, the tensile strains recorded under standard axle loads were greater than those recorded under light axle loads, which is consistent with the evidences that fatigue damage is dominated by the heavy traffic loads.
- The tensile strains in all test sections were found to decrease with increasing asphalt thickness (and/or asphalt quality), irrespective of presence or absence of geosynthetic reinforcements.
- The traffic-induced tensile strains in the three geosynthetic-reinforced sections evaluated in this study were consistently lower than those in the control section, irrespective of the axle loads and the pavement configurations. Specifically, tensile strain reductions in geosynthetic-reinforced sections, in relation to the control section,

exceeded 45% and 25% for Pavement Configurations A and B, respectively.

- The tensile strain reduction ratios ranged from 0.38 to 0.53 and from 0.60 to 0.73 for standard axle loadings applied on 50 mm-thick and 75 mm-thick asphalt overlays, respectively.
- The tensile strain reduction ratios ranged from 0.44 to 0.59 and from 0.53 to 0.75 for light axle loadings applied on 50 mm-thick and 75 mm-thick asphalt overlays, respectively.
- These trends indicate that the tensile strain reduction ratios are affected by the pavement configuration (e.g., thickness and type of the asphaltic layer), traffic load magnitudes, and also the ambient air and asphalt temperatures during the loadings.

Overall, the geosynthetic-reinforced sections considered in this study were found to perform clearly better than the control section in terms of minimizing the tensile strains under standard and light axle loads and, consequently, enhancing the structural capacity of the pavement system. This finding may have significant practical implications, considering that geosynthetic interlayers are often included below the asphalt overlays with the objective of minimizing reflective cracking rather than increasing the structural capacity of the flexible pavement. While the future performance of the test sections also helps evaluating the effectiveness of the different geosynthetic interlayers to minimize reflective cracking, such evaluation is beyond the objectives of this study. Ultimately, the use of geosynthetic reinforcements in asphalt overlays may result in reduction in the asphalt thickness and/or in an extension in the service life of geosynthetic-reinforced overlay sections.

Acknowledgements

The authors wish to thank the Texas Department of Transportation (TxDOT) for the financial support received for this study. Special thanks are due to Giselle Carrasco and Mike Arellano from the Austin District.

References

Abdesssemed, M., Kenai, S., Bali, A., 2015. Experimental and numerical analysis of the behavior of an airport pavement reinforced by geogrids. Construct. Build. Mater. 94, 547–554.
ASTM D5261, 2018. Standard Test Method for Measuring Mass Per Unit Area of Geotextiles. Annual Book of ASTM Standards, ASTM International, West Conshohocken, PA, USA.
ASTM D6140, 2014. Standard Test Method to Determine Asphalt Retention of Paving Fabrics Used in Asphalt Paving for Full-Width Applications. Annual Book of ASTM Standards, ASTM International, West Conshohocken, PA, USA.
ASTM D6637, 2015. Standard Test Method for Determining Tensile Properties of Geogrids by the Single or Multi-Rib Tensile Method. Annual Book of ASTM Standards, ASTM International, West Conshohocken, PA, USA.
Buhler, A., 2007. Study the Effect of Grid Reinforcement in Pavement Restoration. PhD Thesis Submitted to ITA. Sao Jose dos Campos, Sao Paulo, Brazil.
Canestrari, F., Cardone, F., Gaudenzi, E., Chiola, D., Gasbarro, N., Ferrotti, G., 2022. Interlayer bonding characterization of interfaces reinforced with geocomposites in field applications. Geotext. Geomembranes 50 (1), 154–162.
Cleveland, G.S., Button, J.W., Lytton, R.L., 2002. Geosynthetic in Flexible and Rigid Pavement Overlay. Texas Transport Institute, Texas A&M University System. Report 1777-1.
Correia, N.S., Zornberg, J.G., 2016. Mechanical response of flexible pavements enhanced with geogrid-reinforced asphalt overlays. Geosynth. Int. 23 (3), 183–193.
Correia, N.S., Zornberg, J.G., 2018. Strain distribution along geogrid-reinforced asphalt overlays under traffic loading. Geotext. Geomembranes 46, 111–120.
Correia, N.S., Esquivel, E.R., Zornberg, J.G., 2018. Finite-element evaluations of geogrid-reinforced asphalt overlays over flexible pavements. J. Transport. Eng., Part B: Pavements 144 (2), p. 04018020.
Elseifi, M.A., 2003. Performance Quantification of Interlayer Systems in Flexible Pavements Using Finite Element Analysis, Instrument Response and Non Destructive Testing. PhD Thesis. submitted to Virginia Polytechnic Institute and State University, Virginia, USA.
Farshad, A., 2005. Potential Applications of Paving Fabrics to Reduce Reflective Cracking. Jackson State University, Mississippi, Federal Highway Report. FHWA/MS-DOT-RD-2005-174.
Ferrotti, G., Canestrari, F., Pasquini, E., Virgili, A., 2012. Experimental evaluation of the influence of surface coating on fiberglass geogrid performance in asphalt pavements. Geotext. Geomembranes 34, 11–18.
Gonzalez-Torre, I., Calzada-Perez, M.A., Vega-Zamanillo, A., Castro-Fresno, D., 2015. Experimental study of the behavior of different geosynthetics as anti-reflective cracking systems using a combined-load fatigue test. Geotext. Geomembranes 43, 345–350.
Graziani, A., Pasquini, E., Ferrotti, G., Virgili, A., Canestrari, F., 2014. Structural response of grid-reinforced bituminous pavements. Mater. Struct. 47 (8), 1391–1408.
Imjai, T., Pilakoutas, K., Guadagnini, M., 2019. Performance of geosynthetic-reinforced flexible pavements in full-scale field trials. Geotext. Geomembranes 47, 217–229.
Kazimierowicz-Frankowska, K., 2020. Influence of geosynthetic reinforcement on maximum settlements of semi-rigid pavements. Geosynth. Int. 27 (4), 348–363.
Kumar, V.V., Roodi, G.H., Zornberg, J.G., 2021c. Asphalt strain response of geosynthetic-reinforced asphalt overlays under static plate loads. In: Proceedings of Geosynthetics Conference 2021. Kansas city, Kansas, USA, pp. 350–361.
Kumar, V.V., Saride, S., 2017. Evaluation of Flexural Fatigue Behavior of Two-Layered Asphalt Beams with Geosynthetic Interlayers Using Digital Image Correlation. *Proceedings of the Transportation Research Board 96th Annual Meeting*, Washington DC, USA, pp. 8–12.
Kumar, V.V., Saride, S., Zornberg, J.G., 2021a. Fatigue performance of geosynthetic-reinforced asphalt layers. Geosynth. Int. 28 (6), 584–597. https://doi.org/10.1680/jgein.21.00013.
Kumar, V.V., Saride, S., Zornberg, J.G., 2021b. Mechanical response of full-scale geosynthetic-reinforced asphalt overlays subjected to repeated loads. Transport. Geotech. 30, 100617. https://doi.org/10.1016/j.trgeo.2021.100617.
Kwon, J., Tutumluer, E., Kim, M., 2005. Development of a mechanical model for geosynthetic-reinforced flexible pavements. Geosynth. Int. 12 (6), 310–320.
Laurinavicius, A., Oginskas, R., 2006. Experimental research on the development of rutting in asphalt concrete pavements reinforced with geosynthetic materials. J. Civ. Eng. Manag. 12 (4), 311–317.
Lytton, R.L., 1989. Use of geotextiles for reinforcement and strain relief in asphalt concrete. Geotext. Geomembranes 8 (3), 217–237.
Pasquini, E., Bocci, M., Canestrari, F., 2014. Laboratory characterization of optimized geocomposites for asphalt pavement reinforcement. Geosynth. Int. 21 (1), 24–36.
Roodi, G.H., Morsy, A.M., Zornberg, J.G., 2017. Experimental evaluation of the interaction between geosynthetic reinforcements and hot mix asphalt. In: Proceedings of the International Conference on Airfield and Highway Pavements. ASCE, Philadelphia, Pennsylvania, USA, pp. 428–439.
Sanders, P.J., 2001. Reinforced Asphalt Overlays for Pavements. PhD Thesis. submitted to the University of Nottingham, UK.
Saride, S., Kumar, V.V., 2017. Influence of geosynthetic-interlayers on the performance of asphalt overlays on pre-cracked pavements. Geotext. Geomembranes 45 (3), 184–196.
Saride, S., Kumar, V.V., 2019. Estimation of service life of geosynthetic-reinforced asphalt overlays from beam and large-scale fatigue tests. J. Test. Eval. 47 (4), 2693–2716.
Siriwardane, H., Gondle, R., Bora, K., 2010. Analysis of flexible pavements reinforced with geogrids. Geotech. Geol. Eng. 28 (3), 287–297.
Solatiyan, E., Bueche, N., Carter, A., 2020. A review on mechanical behavior and design considerations for reinforced-rehabilitated bituminous pavements. Construct. Build. Mater. 257, 119483. https://doi.org/10.1016/j.conbuildmat.2020.119483.
Solatiyan, E., Bueche, N., Carter, A., 2021. Laboratory evaluation of interfacial mechanical properties in geogrid-reinforced bituminous layers. Geotext. Geomembranes 49 (4), 895–909.
Spadoni, S., Ingrassia, L.P., Paoloni, G., Virgili, A., Canestrari, F., 2021. Influecne of geocomposite properties on the crack propagation and interlayer bonding of asphalt pavements. Materials 14 (8), 5310. https://doi.org/10.3390/ma14185310.
Sudarsanan, N., Karpurapu, R., Amrithalingam, V., 2019. Investigations on fracture characteristics of geosynthetic reinforced asphalt concrete beams using single edge notch beam tests. Geotext. Geomembranes 47 (5), 642–652.
TxDOT, 2014. Standard Specifications for Construction and Maintenance of Highways, Streets, and Bridges. Texas Department of Transportation (TxDOT), Austin, Texas, USA.
Virgili, A., Canestrari, F., Grilli, A., Santagata, F.A., 2009. Repeated load test on bituminous systems reinforced by geosynthetics. Geotext. Geomembranes 27, 187–195.
Wathugala, G.W., Huang, B., Pal, S., 1996. Numerical simulation of geosynthetic-reinforced flexible pavements. Trans. Res. Rec. J. Transport. Res. Board 1534, 58–65.
West, R.C., Zhang, J., Moore, J., 2005. Evaluation of Bond Strength between Pavement Layers. NCAT Report 05-08. National Center for Asphalt Technology, Auburn, Alabama, USA.
Zamora-Barraza, D., Calzada-Perez, M.A., Castro-Fresno, D., Vega-Zamanillo, A., 2011. Evaluation of anti-reflective cracking systems using geosynthetics in the interlayer zone. Geotext. Geomembranes 29 (2), 130–136.
Zornberg, J.G., 2017. Functions and applications of geosynthetics in roadways. Procedia Eng. 189, 298–306.